Annals of Biomedical Engineering, Vol. 28, pp. 781–792, 2000
Printed in the USA.

0090-6964/2000/28(7)/781/12/$15.00

Three-Dimensional Stress and Strain in Passive Rabbit Left Ventricle: A Model Study

FREDERICK J. VETTER and ANDREW D. MCCULLOCH

Department of Bioengineering, University of California San Diego, San Diego, CA

(Received 13 July 1999; accepted 12 June 2000)

Abstract—To determine regional stress and strain distributions in rabbit ventricular myocardium, an anatomically detailed finite element model was used to solve the equations of stress equilibrium during passive filling of the left ventricle. Computations were conducted on a scalable parallel processing computer and performance was found to scale well with the number of processors used, so that stimulations previously requiring approximately 60 min were completed in just over 5 min. Epicardial strains from the model analysis showed good agreement (RMSE = 0.007332) with experimental measurements when material properties were chosen such that cross fiber strain was more heterogeneous than fiber strain, which is also consistent with experimental observations in other species. © *2000 Biomedical Engineering Society.*
[S0090-6964(00)00507-5]

Keywords—Ventricular mechanics, Scalable parallel computation, Finite element analysis.

INTRODUCTION

The three-dimensional geometry and fiber orientation of the intact myocardium plays an important role in the diastolic mechanics of the ventricles. Previous models of passive mechanics have simulated the canine and rat left ventricles.[3,6,19,26] Yet no models have analyzed stress and strain in the rabbit ventricles even though this species is a popular model for the study of mechanics, mechanoenergetics, and electrical propagation.[10,11,23,33]

Two-dimensional epicardial strains were measured in the rabbit left ventricle (LV) by Gallagher *et al.*[10] to study the changes of collagen fiber structure and mechanics of the cardiac scar after infarction. They measured LV volume, fiber orientation, and fiber, cross fiber, and shear strains on the anterolateral epicardium of isolated hearts from a control group, and from groups at 3 and 14 d postinfarction under passive LV pressure loads of 0–30 mm Hg. In the control group, fiber strain was consistently larger than cross fiber strain and accompanied by a small negative shear strain, characteristics similar to epicardial strains measured in rat, canine, and porcine hearts.[15,27,26]

Despite experimental evidence that left ventricular wall mechanics are three dimensional,[31] only a few fully three-dimensional mechanics models exist. Huyghe *et al.*[19] have developed an axisymmetric quasilinear viscoelastic finite element (FE) model of the canine LV incorporating ventricular torsion, transmural fiber anisotropy, and intracoronary blood in the wall. Bovendeerd *et al.*[3] have studied the effects of ischemia on the border zone mechanics, stroke work, and global deformation using a three-dimensional LV model featuring the dependence of active fiber stress on time, strain, and strain rate.

Mechanics models based on simplified LV geometries have been useful for gaining basic insights into the importance of the thick LV wall geometry, torsional deformation, large elastic deformation, and transverse shear strains.[14,17] These models, however, cannot account for the complex three-dimensional variations in wall thickness, curvature, or fiber orientation in the analysis of stress or strain in the ventricle. Furthermore, simplified models do not allow for interactions between the left and right ventricles (RV), the pericardium, or coronary blood flow. Hence more sophisticated models of the ventricles, incorporating a realistic three-dimensional geometry and fiber architecture, a constitutive law reflecting the nonlinear anisotropic elastic properties of myocardium, and boundary conditions that impose physiologically realistic constraints under normal or diseased conditions are required for studying the heterogeneous regional mechanics of intact myocardium. These three-dimensional anatomically detailed models require large-scale computation. Fortunately, advances in parallel computing hardware and software have made large-scale three-dimensional models of cardiac mechanics feasible. Our goal was to estimate the material parameters of intact rabbit LV myocardium using measurements of epicardial strain and an accurate three-dimensional model of

Frederick J. Vetter is currently with the Department of Pharmacology, SUNY Upstate Medical University, Syracuse NY.

Address correspondence to Andrew D. McCulloch, Department of Bioengineering, University of California San Diego, 9500 Gilman Drive, La Jolla, CA 92093-0412. Electronic mail: mcculloc@bioeng.ucsd.edu

ventricular geometry and fiber orientation. We expected a parallel processing approach would be necessary to reduce the simulation run times to a point where exploration of the parameter space was feasible.

Anatomic Model

The anatomic model of the rabbit ventricular geometry and fiber architecture described by Vetter and McCulloch[30] was modified to serve as a computational domain for the model of passive LV inflation simulating the control group experiments of Gallagher *et al.*[10] The discontinuous fitted fiber orientations allowed by extra nodes at the junction of the RV septal and free wall surfaces were removed to avoid numerical difficulties by assigning the average fiber orientation at the redundant nodes along the junction to a single node, and removing the redundant nodes. A small apical hole ($\mu = 1°$) was introduced to eliminate redundant nodes in this region. The mesh was converted from prolate spheroidal to rectangular Cartesian coordinates so that the deforming model could admit translations at the apex. This conversion required two circumferential refinements of the FE mesh on the left ventricular free wall to maintain the geometry in the region of the LV papillary muscle insertions. The resulting 48-element mesh was used as the computational domain for simulating passive inflation of the LV.

The FE model used tricubic Hermite interpolation functions with four point Gaussian quadrature integration in each of the local FE directions. Because no analytic solution exists for this problem, convergence of the FE mesh was determined asymptotically: the 48-element model was inflated to 5 mm Hg, and regions of highest strain energy were refined until the overall strain energy of the deformed mesh changed by less than 0.5%. This resulted in a 174-node model (9 circumferential×5 longitudinal×2 transmural elements) with 4176 degrees of freedom (DOF;8 DOF per variable per node×3 variables×174 nodes), suitable for modeling the three-dimensional deformation of rabbit ventricular myocardium. The LV of the 90-element model was inflated from 0 to 25 mm Hg in 5 mm Hg increments, with 5 load steps per increment (6 load steps for the 5–10 mm Hg increment). The RV was unloaded throughout the simulation to approximate the experimental protocol followed by Gallagher *et al.*[10]

Constitutive Law

The myocardium was modeled as a transversely isotropic, hyperelastic material with an exponential strain energy function[14,27]

$$W = \tfrac{1}{2}C(e^{Q} - 1),$$

$$Q = b_1 E_{ff}^2 + b_2(E_{rr}^2 + E_{cc}^2 + 2E_{rc}^2) + 2b_3(E_{fr}^2 + E_{fc}^2), \quad (1)$$

where the Lagrangian Green's strains E_{ij} are referred to the local fiber coordinate system consisting of fiber (f), cross fiber (c), and radial (r) coordinate directions. The material parameters C, b_1, b_2, and b_3 have been described in detail elsewhere;[14] briefly, the material constant C scales the stress, b_1 or b_2 scales the material stiffness in the fiber or cross fiber direction, respectively, and b_3 scales the material rigidity under shear in the fiber-radial and fiber-cross fiber planes.

Treating the kinematic incompressibility constraint explicitly as an additional equation results in a mixed formulation that makes numerical solution difficult unless a memory-intensive direct solution method is used. Instead, we introduced a bulk modulus parameter b_4 into the strain energy[25]

$$W = \tfrac{1}{2}C(e^{Q} - 1) - b_4(\det[\mathbf{C}] - 2\sqrt{\det[\mathbf{C}]} + 1), \quad (2)$$

where $\det[\mathbf{C}]$ is the determinant of the right Cauchy–Green deformation tensor. As described previously,[25] this approach is equivalent to a penalty formulation for incompressibility since experimental estimates of the bulk modulus parameter b_4 are large compared with the other coefficients (200 kPa).[35] The material parameters C, b_1, b_2, and b_3 in Eq. (2) were estimated so that the Lagrangian Green's strain components E_{ff}, E_{cc}, and E_{fc} agreed with epicardial strain measurements from the isolated, arrested rabbit heart as reported by Gallagher *et al.*[10]

LV passive inflation was simulated, strains were compared with experimental measurements, and material parameters were adjusted to improve the agreement: b_1 and b_2 were modified to minimize discrepancies in fiber and cross fiber strains and b_3 was modified according to differences in shear strain. We computed the root mean squared error (RMSE) of the objective function

$$\hat{E}_{ij} - E_{ij},$$

where $\hat{E}_{ij}$ were the model strains and E_{ij} are the epicardial strains measured by Gallagher *et al.*[10] at LV pressures of 5, 10, 15, 20, and 25 mm Hg. The parameters that minimized the RMSE were accepted as the best estimates of myocardial material parameters.

Boundary Conditions

Boundary conditions were specified by constraining the nodal displacement degrees of freedom. Nodal derivatives are with respect to the arc length S_i in the physical coordinate direction x_i.[24] Nodal coordinates and

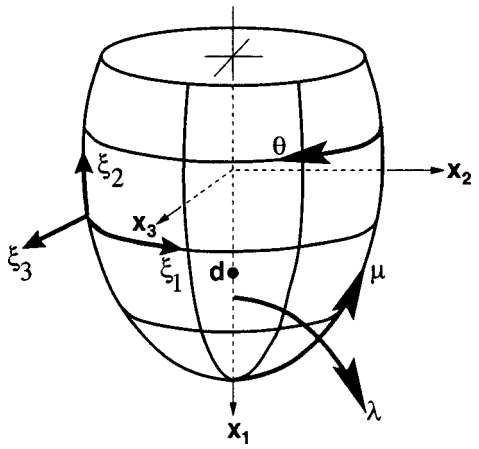

FIGURE 1. Schematic diagram of the rectangular Cartesian model coordinate system (x_1, x_2, x_3) is collinear with the long axis of the LV cavity. The prolate spheroidal coordinate system (λ, μ, θ) is convenient for modeling cardiac geometry. The curvilinear parametric coordinates (ξ_1, ξ_2, ξ_3) are the local finite element coordinates.

their circumferential and transmural derivatives were constrained at the base on the epicardium and right ventricular endocardium to approximate the effects of the relatively stiff annuli of the valves. The LV endocardium at the base was constrained to move only in the basal plane, allowing cavity expansion but not longitudinal displacement in the x_1 direction. At the apex all derivatives in the posterior direction and nodal coordinates were unconstrained. Constraints to the longitudinal and transmural derivatives at the apex prevented spurious solutions with unrealistically large deformations along the boundary of the small apical hole, and were imposed only to improve the behavior of the model and not as an attempt to achieve any type of symmetry or regionally uniform response. Referring to the coordinate systems in Fig. 1, the nodal displacement constraints used here are expressed mathematically as

$\delta v = 0$ at the epicardial base and RV endocardial base (physical units of mm),

$$\delta \frac{\delta v}{\partial S_1} = \delta \frac{\delta v}{\partial S_2} = 0$$

at the epicardial base, RV endocardial base, and LV endocardial apex (dimensionless),

$$\delta \frac{\partial v}{\partial S_2} = 0$$ at the LV endocardial apex (dimensionless),

$$\delta \frac{\partial^2 v}{\partial S_1 \partial S_2} = 0$$ at the epicardial base, RV endocardial base, and LV endocardial apex (mm^{-1}),

$$\delta \frac{\partial^2 v}{\partial S_2 \partial S_3} = 0$$ at the LV endocardial apex (mm^{-1}),

$$\delta \frac{\partial^3 v}{\partial S_1 \partial S_2 \partial S_3} = 0$$ at the epicardial base and LV endocardial apex (mm^{-2}),

where v is one of the three spatial coordinates: $v \in \{x_1, x_2, x_3\}$. At the LV endocardial base the following constraints allowed cavity expansion but prevented longitudinal displacement:

$$\delta x_1 = 0,$$

$$\delta \frac{\partial x_1}{\partial S_1} = \delta \frac{\partial x_1}{\partial S_3} = 0,$$

$$\delta \frac{\partial^2 x_1}{\partial S_1 \partial S_3} = 0.$$

These boundary conditions removed 393 DOFs from the 90 element model, leaving 3783 DOFs to be determined via the FE method.

Computational Approach

To implement the FE method on a scalable parallel processing (SPP) computer, an ''element-by-element'' formulation was used in which the global stiffness matrix **K** is not explicitly assembled.[16] Instead, each processor maintained its assigned element stiffness matrices and was responsible for providing any information in the global stiffness derived from these element stiffness matrices.

An iterative method was used to solve the linear systems of equations. It is important at this point to distinguish between the two iterative approaches that were utilized: the iterations of the Newton–Raphson method were part of the process to determine the solution for the nonlinear system. The iterative methods described here solve the linear systems that arise as approximations within each Newton–Raphson iteration. Such a method will perturb an initial guess of the global solution $\tilde{u}$ based on a search criteria specific to a particular iterative method. We chose the restarted Generalized Minimal Residual (GMRES) method as implemented in the Parallel Iterative Methods (PIM) package.[8] Unlike other implementations of iterative methods,[18,21,28] the PIM package places no restrictions on the underlying data structure of the system matrix, requiring instead that the user develop additional support routines for the parallel computation of a matrix–vector product, vector inner product, norm, and global accumulation. For the simulations conducted here, the restarted GMRES method used

100 subspace basis vectors (as described below), a solution tolerance of 10^{-9}, and a maximum of ten restarts. Yeckel and Derby[34] have shown it is not always advantageous to solve the linear system to a high degree of precision as long as the nonlinear Newton iteration converges to an acceptable tolerance. We adopted their strategy and allowed the Newton iteration to advance even when the restarted GMRES method had executed the maximum number of restarts. All components of $\hat{u}$, the approximation of the global solution vector $\tilde{u}$, were initially set to unity. The solution was accepted when the change in strain energy was less than 10^{-6} kPa.

Material parameters of the passively inflated rabbit LV were estimated using the recently proposed form of the constitutive law [Eq. (1)]. The element-by-element approach was implemented on a SPP computer to reduce run time, and a modified Newton–Raphson method was used to solve the nonlinear system of equations, utilizing the restarted GMRES method to solve the linear systems of equations during each modified Newton–Raphson iteration. The strategy implemented here requires only that the diagonal preconditioner, the solver residual vector, and partial products of the element stiffness matrices with either the diagonal preconditioner or intermediate solver vectors be globally reduced and broadcast to all processors. We balanced the computational load by assigning an equal number of FEs to each available processor. We expected this approach to be highly scalable (i.e., speedup would increase in proportion to the number of processors). We computed speedup as the run time on a single processor divided by the run time on P processors. Our implementation used the Message Passing Interface library on the Cray T3E (272 processors running at 300 MHz, each with 128 Mbyte of main memory) at the San Diego Supercomputer Center.

The computational problem and solution parameters were defined on a laboratory work station (SGI Indigo^2). The contents of the global data structures were then written to a binary file (approximately 8.7 Mbyte), which was then transferred to the Cray T3E via the UNIX file transfer protocol (ftp). On the T3E, the parallel version of the program was launched on 45 processors, each of which read the binary file and loaded the global data into memory. Assigning static global data in this manner obviated several one-to-all broadcasts, greatly simplifying the problem definition on the SPP computer. At the start of the first solution procedure, each processor determined which of the element stiffness matrices it was to compute and store—with 45 processors and a mesh with 90 finite elements, each processor computed and stored two of the 90 element stiffness matrices and carried a copy of the current approximate solution vector $\hat{u}$. When the restarted GMRES algorithm required an evaluation of the matrix–vector product $\mathbf{K}\hat{u}$, each processor mapped the subset of relevant components in the approximate solution vector $\hat{u}$ to the appropriate columns in the element stiffness matrix and executed the multiplication. The resulting 45 vectors of partial products were summed across the processors to form the full matrix–vector product $\mathbf{K}\hat{u}$. The current approximation $\hat{u}$ was then updated by the restarted GMRES algorithm to form the subsequent approximation to the global solution $\hat{u}$. After the global solution was obtained, the root processor wrote the nodal parameters of the deformed configuration, cavity pressure, and global residual vector to output files (approximately 860 kbyte per load step). If the simulation was to continue to higher LV pressures the solution procedure was repeated, otherwise the program was terminated normally on all processors. When the simulation was completed the output files were transferred to a laboratory work station for analysis and visualization.

RESULTS

Validation: Canine LV Passive Inflation

A high-order FE model of the canine LV (described elsewhere[6]) with 960 DOFs served to validate the parallel implementation of the finite element procedures. Using the constitutive law in Eq. (2) with material parameters[6] $C=1.76$ kPa, $b_1=18.5$, $b_2=3.58$, $b_3=1.63$, and $b_4=30$, the LV was inflated to 7.5 mm Hg in four successive load steps, using either a full Newton method or a modified Newton–Raphson method. Left diagonal preconditioning reduced the condition number (i.e., the ratio of the magnitudes of the largest and smallest eigenvalues) of the global tangent stiffness matrix from 550×10^6 to 3,570; without preconditioning the restarted GMRES method never reduced the residuals and always failed to converge. The restarted GMRES subspace had 100 basis vectors, approximately the number resulting in the minimum run time. The solution was identical to that reported previously.[6] The resulting run times and speedup are shown in Fig. 2. On 16 processors run time was reduced to 8.7 min using the full Newton method, or to 5.2 min using a modified Newton–Raphson method. With the full Newton method speedup was 13.9, but only 10.6 with the modified Newton–Raphson method. The full Newton method required 23 evaluations of the global tangent stiffness matrix **K** and 116 restarted GMRES iterations, whereas the modified Newton–Raphson method required six evaluations of **K** and 383 restarted GMRES iterations.

Rabbit LV Passive Inflation

Computation. Twelve simulations (3783 DOFs) were conducted to determine the best estimates of the material parameters; the results presented here are from the simulation using the best estimates. The number of iterations

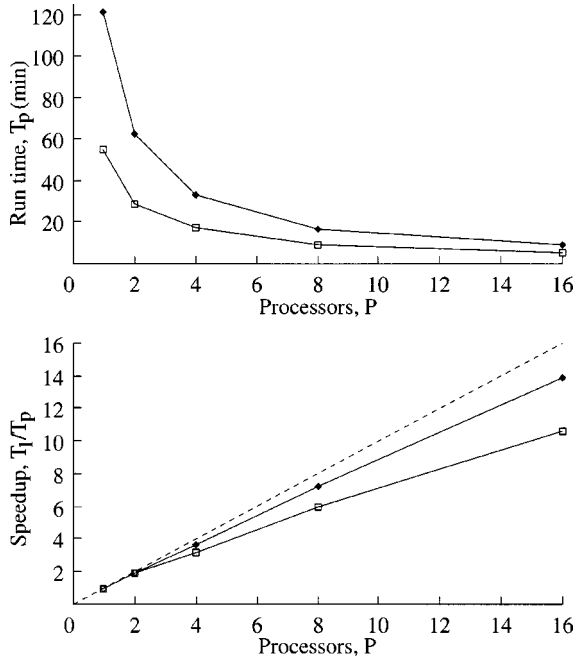

FIGURE 2. Run time and speed up for the 16 element canine LV simulation (see Ref. 6) using either a full Newton (diamonds) or modified Newton–Raphson (boxes) method. Dashed line is ideal speedup. Using 16 processors resulted in 87% efficiency for the full Newton method, and 66% efficiency for the modified Newton–Raphson method.

and execution times for each LV pressure range are shown in Table 1. On 45 processors this simulation required 237.5 CPU hours and ran for approximately 5.3 h. On each processor data storage required 14.4 Mbyte of main memory and the program required 9.84 Mbyte of main memory.

Global Deformation of the Ventricles. A cross section of the unloaded and deformed ventricles at 25 mm Hg LV pressure (Fig. 3, left) shows the LV cavity volume increased substantially and the apex displaced 2.18 mm in the longitudinal direction, flattening the septal wall. At 5 and 25 mm Hg pressure the septum was displaced 2.0 and 3.7 mm toward the RV at the equator. The RV cavity maintained a volume of at least 1 ml throughout the pressure range and the LV cavity volume was was within 10% of the experimentally measured volumes at nonzero pressures (Fig. 3, right).

Epicardial and Transmural Strains. When parameters of the strain energy function had the the values $C=1.76$, $b_1=50.0$, $b_2=5.0$, $b_3=1.63$, $b_4=200$, the model showed good agreement (RMSE=0.007332) with epicardial strains measured on the anterolateral wall (Fig. 4, top).[10] The fiber and cross fiber strains were well within the error of the experimental measurements, but the magnitude of the fiber-cross fiber shear strain is larger than

TABLE 1. Number of Newton–Raphson iterations and run time required to simulate the passive inflation of the rabbit LV from 0 to 25 mm Hg. Preliminary simulations showed the nonlinear solver diverged using five load steps for the 5–10 mm Hg range. Six load steps were used to provide a smaller load increment for each step over this range.

LV pressure (mm Hg):	0–5	5–10	10–15	15–20	20–25
Load step 1:	11	17	13	15	13
2:	10	11	11	10	7
3:	11	11	11	9	9
4:	13	13	10	10	9
5:	11	10	8	10	7
6:		9			
Total Newton–Raphson iterations:	56	71	53	54	45
Run time (s):	4155	5484	3771	3830	2990

that of experiment by an average of 12%, suggesting the elastic stiffness of the model in the tangent plane [parameter b_3 in Eq. (2)] may be lower than that in the actual rabbit LV myocardium. This is further highlighted in the principal strain profiles and direction of the first principal strain (Fig. 5, top), where the first principal strain is consistently larger than experiment, the maximum difference occurring at 25 mm Hg pressure where the strain computed from the experimental data is 0.075 but the model predicted 0.088. Similarly, the second principal strain is consistently lower than experiment with the largest discrepancy at 10 mm Hg pressure (measured: 0.014; model: 0.0098). The direction of the first principal strain in the model closely followed that computed from the experimental measurements (Fig. 5, bottom), and in both cases the direction was more negative than the local epicardial fiber angle (in the experimental hearts the mean local epicardial fiber angle is $-60°$, in the model the angle was $-52°$). The largest error is at 5 mm Hg pressure where the angle computed from the experimental data is $-68°$, but the model yielded $-78°$. In addition, variations of the first principal strain direction with increasing LV pressure differ slightly: the experimental data show the direction becoming monotonically more longitudinal with increasing LV pressure; in the model the change in direction shifted from negative to positive at pressures above 15 mm Hg.

At 25 mm Hg LV pressure, fiber strain varied from 0.012 to 0.093 at the subepicardium and from 0.04 to 0.14 at the subendocardium (Fig. 6). Conversely, cross-fiber strain shows a much larger transmural variation: -0.002 to 0.22 strain at the subepicardium and -0.016 to 0.43 at the subendocardium. The compressive strains were isolated to a single region near the LV posterior papillary insertion (the lighter regions in the lower right portion of the cross fiber strain maps in Fig. 6).

The transmural variation in strain at 10 mm Hg from the same anterolateral region (Fig. 7) showed that both

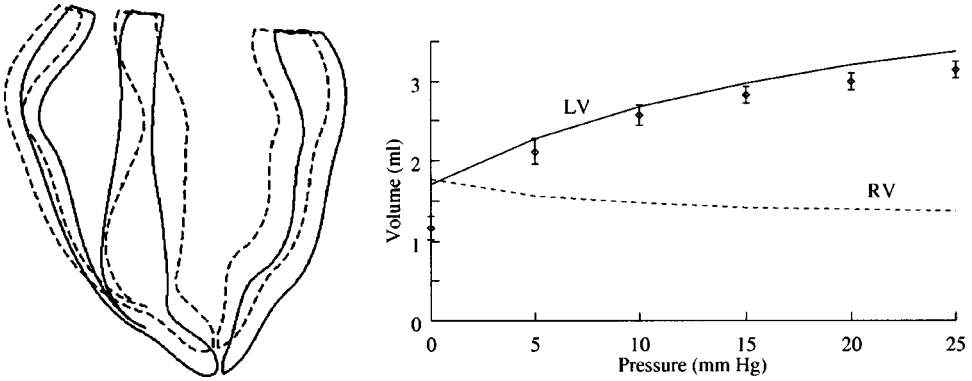

FIGURE 3. (Left) Anterior view of the unloaded (dashed line) and deformed (solid line) ventricular cross-sections at 25 mm Hg. (Right) Measured LV cavity volume [symbols±standard error of the mean (SEM) (Ref. 10)] and LV and RV volumes from the model.

circumferential and radial strains increase in magnitude toward the endocardium, similar to strains measured in the passively inflated (8 ± 4 mm Hg) canine LV.[26] The radial strain was negative because the wall thinned under pressure loading with the greatest amount occurring at the subendocardium. The longitudinal strain, however, remained relatively uniform through the wall (0.045 ± 0.012). Overall, the circumferential–longitudinal shear strain was small and negative through the wall (-0.018 ± 0.011) but became positive at 95% wall depth, with a value of 0.011 at the endocardium. The circumferential–radial shear was negative throughout the the wall (-0.086 ± 0.031) and the longitudinal–radial shear rapidly became most negative (-0.081) at 66% wall depth, then sharply increased to a maximum ($+0.218$) at the endocardial surface.

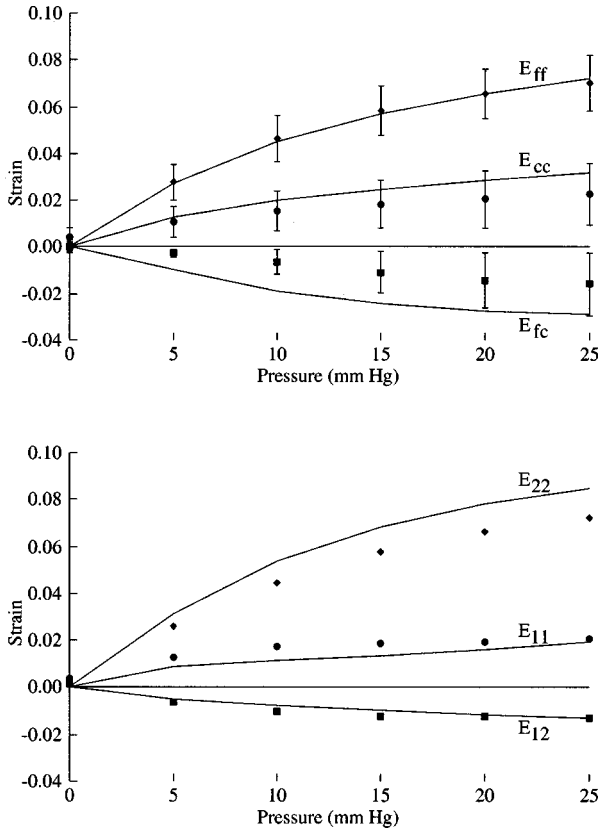

FIGURE 4. Epicardial strain profiles from the anterolateral wall (top). Simulations (lines) show good agreement with experimental fiber (diamonds), cross fiber (circles), and shear (boxes) strains (Ref. 10). Error bars are ± SEM. Epicardial strains from the same region in cardiac coordinates (bottom). Simulations (lines) show good agreement with experimental circumferential (circles), longitudinal (diamonds), and shear (boxes) strains.

Regional LV Wall Stress. Over the lateral wall and apex, Cauchy stress resolved in the fiber direction was on average higher than that in the cross-fiber direction; for the region shown in Fig. 8 the mean fiber stress was 2.91 ± 3.93 kPa and the mean cross fiber stress was 1.47 ± 3.51 kPa. At the midventricle fiber stress tended to be

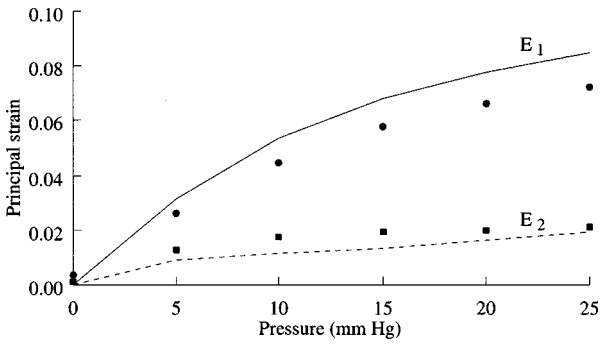

pressure:	5	10	15	20	25	mm Hg
experiment:	−68.4	−71.2	−74.1	−75.9	−76.9	degrees
model:	−78.6	−80.0	−80.0	−79.8	−79.4	degrees

FIGURE 5. Principal strain profiles (top) and angle (bottom) from the epicardial surface on the anterolateral wall. Simulation (line) shows good agreement with experimental strains (symbols) (see Ref. 10).

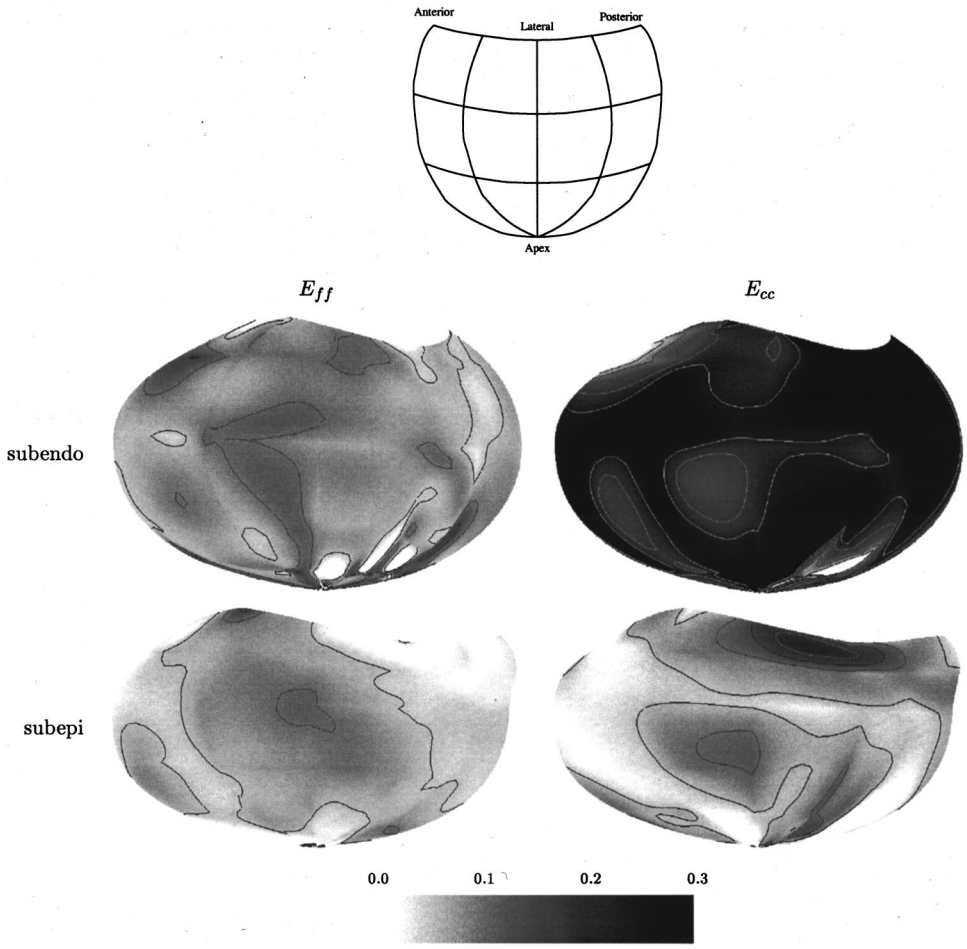

FIGURE 6. Hammer projection maps of fiber strain (left) and cross fiber strain (right) in the LV free wall at 25 mm Hg pressure. Contours are drawn at 0.05, 0.10, 0.15, 0.20, and 0.25 strain levels.

larger than cross fiber stress transmurally. At the epicardium and midwall, cross-fiber stress was more uniform than the fiber stress, although fiber stress tended to be larger. The apex and papillary insertions at the subendocardium show the greatest magnitude and regional variability in both directions, where negative stresses occurred predominately at the regions of negative curvature.

DISCUSSION

Simulations of passive LV inflation were conducted using a realistic model of the rabbit ventricles. Material parameters of a transversely isotropic, hyperelastic constitutive law were found that predicted epicardial strains in the anterolateral wall which were consistent with experiment. These results further the understanding of the passive mechanics of the intact rabbit ventricular myocardium, and may be important when interpreting the results of experimental investigations in mechanics,[10] mechanoenergetics,[33] or electrical propagation.[11]

High-order FE models have been used previously to investigate ventricular mechanics. Some assume an axisymmetric geometry that cannot model regional variations in stress due to local variations in wall thickness or curvature.[19,20] Others have assumed constant transmural variation in fiber orientation or lack the right ventricle.[1,6] A high-order FE model of the canine left and right ventricles has been developed[24] but its use in modeling ventricular mechanics has been limited.[5] The model used here features an anatomically accurate left and right ventricular geometry and a realistic nonuniform transmural variation in fiber orientation. The element-by-element approach to solving the nonlinear system of governing equations was shown to be highly scalable on a parallel processing computer, achieving near-linear speedups for a similar passive inflation problem in the canine LV. Previous simulations requiring 60 min to complete on a laboratory work station were completed here in just over 5 min, a 90% reduction in run time.[6] More importantly, larger and more detailed models can be utilized to obtain new insights regarding myocardial processes and interac-

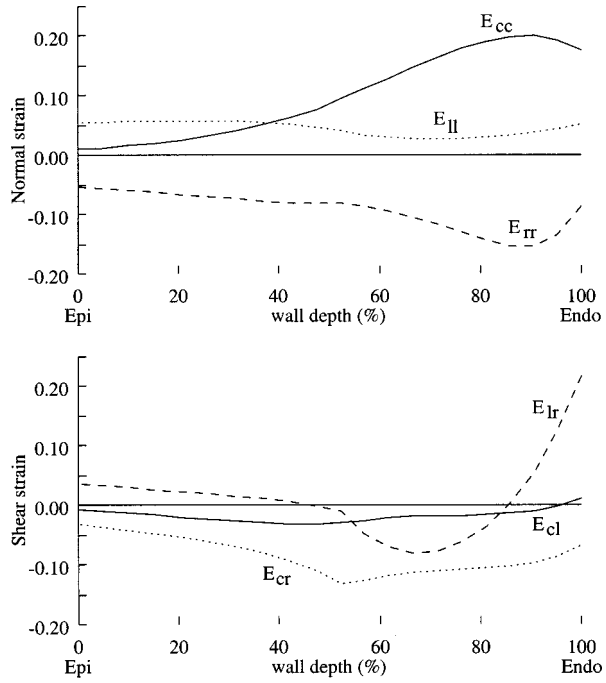

FIGURE 7. Transmural normal and shear strains with respect to cardiac coordinates in the anterolateral region at 10 mm Hg LV pressure. (Top) Circumferential (E_{cc}), longitudinal (E_{ll}), and radial (E_{rr}) strains. (Bottom) Circumferential–longitudinal fiber (E_{cl}), circumferential–radial (E_{cr}), and longitudinal–radial (E_{lr}) shear strains.

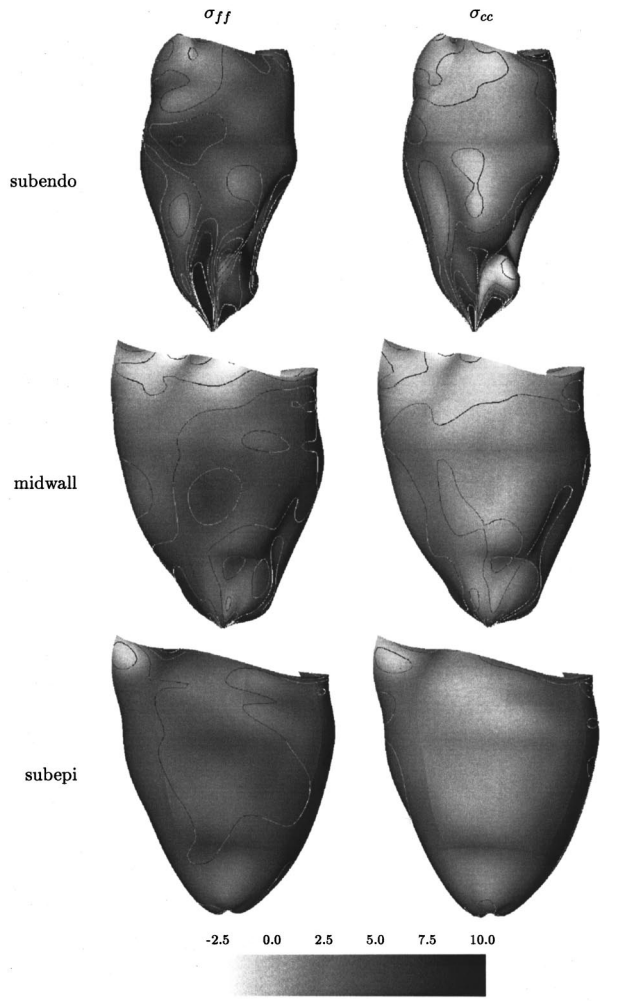

FIGURE 8. Cauchy stress (kPa) resolved in fiber (left) and cross-fiber (right) directions in the LV free wall and apex at 10 mm Hg pressure. Contours are drawn at −2, 0, 2, 4, 6, and 8 kPa stress levels.

tions that are not possible to measure with current experimental techniques.

Computational Approach

In validation runs involving the canine LV simulations, the full Newton method required nearly four times as many evaluations of the global tangent stiffness matrix than did the modified Newton–Raphson method. Evaluation of the global tangent stiffness matrix was an efficient data parallel operation since it required only local data (i.e., information available on the individual processor) to evaluate the element stiffness matrices and no interprocessor communication. The restarted GMRES method, on the other hand, relied heavily on interprocessor communication since partial matrix–vector products must be globally reduced at each iteration. For this phase of the solution procedure the full Newton method required only 116 restarted GMRES iterations, less than one-third of 363 iterations required by the modified Newton–Raphson method. Hence the full Newton method spent proportionally more time executing fully data parallel operations, whereas the modified Newton–Raphson method had a much larger number of synchronization points. Even so, the modified Newton–Raphson method had a shorter run time suggesting that, for this particular problem, evaluation of the global tangent stiffness matrix was more computationally expensive than the interprocessor communication overhead. For a problem where the reverse situation exists using the full Newton method would likely provide shorter run times.

The left diagonal preconditioner we utilized was relatively simple to implement and effective for our problem. Without preconditioning the restarted GMRES method never reduced the residuals and always failed to converge. More elaborate parallel preconditioners exist, however, and would likely accelerate convergence of the restarted GMRES method at the cost of a more complicated implementation. Yeckel and Derby[34] have shown that symmetric left and right diagonal preconditioning is sometimes more effective for accelerating restarted GMRES convergence in computational fluid dynamics problems. Preconditioners based on the individual element stiffness matrices of trilinear brick elements have been shown to be more effective than diagonal scaling,

producing preconditioned systems with substantially lower condition numbers.[32]

Global Deformation of the Ventricles

The global deformation of the model LV reproduces the experimentally measured volumes within 10%,[10] except at the unloaded state (Fig. 3). The initial volume of the model was 1.71 ml, whereas the experimental volume was 1.17 ± 0.39 ml. The disagreement may be due to two factors: one related to the model and the other to the experimental technique. The model omits the LV papillary muscles, and surfaces representing the LV endocardium do not have sufficient spatial resolution to capture the detailed variations on the endocardium;[24] thus it is likely that the model has a higher LV volume than an actual heart. The balloons used to experimentally measure the LV cavity volumes may not completely fill the narrow spaces around the endocardial trabeculae and papillary muscles, resulting in a lower LV volume. These two factors combined may be the cause of the large discrepancy in the unloaded LV volume.

Epicardial and Transmural Strains

During diastole, passive filling of the LV increases cavity volume and distends the ventricular wall. The deformation of the myocardium during filling is highly dependent upon the passive material properties of the myocardium, which are known to vary across species.[26] Characterizing the passive material properties of myocardium is complicated by the complex myofiber arrangement, anisotropy, and nonlinear constitutive relations of the myocardium. Attempts to estimate passive myocardial material properties, however, have been successful in a few cases. Using an exponential form of the constitutive law, Guccione *et al.*[14] have estimated the material properties of passive myocardium in the canine using a cylindrical model of the LV. These material parameters have proven to be effective in reproducing left ventricular strains in the fiber, eross fiber, and radial (transmural) directions in a more realistic prolate spheroidal, high-order FE description of the canine LV.[6] The circumferential–radial and longitudinal–radial components of shear strain, however, did not agree with experimental measurements, suggesting the myocardium may be orthotropic, thus requiring a more detailed mathematical description.[5] Validated orthotropic constitutive laws have not yet been developed, and the transversely isotropic description of three-dimensional passive myocardium has performed sufficiently well in the past.[6]

The longitudinal strain measured in canine LV increased from approximately 0.04 at the epicardium to 0.12 and the subendocardium;[26] in our model, however, longitudinal strain was relatively uniform through the wall. The small positive circumferential–longitudinal shear strain at 95% wall depth indicated the ventricular torsion changed direction (from left-handed to right-handed) at the subendocardium, also at odds with experimental findings. The nonlinear form of the strain-energy function makes it difficult to specify precisely the parameter(s) responsible for this behavior; analyses conducted on similar models with the same strain-energy function suggest the ratio of the fiber stiffness to cross-fiber stiffness parameters b_1/b_2 may influence this result.[14] Similarly, the circumferential–radial shear was negative throughout the wall and the longitudinal–radial shear showed a sudden change in magnitude at the inner third of the wall, neither of which has been observed in the canine or porcine heart.[15,26] These responses of the model could possibly be improved by incorporating material parameters that vary through the wall.[13] The error in the strain components suggests the computed stresses are also in error, although the inaccuracy is difficult to quantify since each component of the three-dimensional stress tensor will depend on all the components of the strain tensor.

Despite these shortcomings, the model accurately predicts epicardial deformation on the anterolateral wall under passive loading. The stiffness in the fiber direction is much greater than in the cross-fiber direction, characteristics similar to those in the canine and rat LV.[27,26] Transmurally, cross-fiber strain showed much greater variation than fiber strain, similar to characteristics found in the canine, but transmural three-dimensional strains have yet to be measured in the intact rabbit ventricle so implications of this result must be derived cautiously.

Regional LV Wall Stress

Lin and Yin[23] recently proposed a constitutive law that is a function of the principal strain invariants for the rabbit ventricular myocardium. Using thin slabs of rabbit myocardium from LV midwall, they measured material deformation in response to a range of applied loads and determined representative material parameters by fitting an exponential form of the strain energy function to data obtained from uniaxial and biaxial tests. Their strain energy function has the form:

$$W = \tfrac{1}{2}C(e^{Q} - 1)$$
$$Q = b_1(I_1 - 3)^2 + b_2(I_1 - 3)(I_4 - 1) + b_3(I_4 - 1)^2, \tag{3}$$

where I_1 is the first strain invariant and I_4 they define as

$$I_4 = \hat{n} \cdot \mathbf{C} \cdot \hat{n},$$

where $\mathbf{C}$ is the right Cauchy–Green deformation tensor and $\hat{n}$ is a unit vector along the muscle fibers in the

TABLE 2. Material parameters used in Eq. (1), (2), or (3) to model the stress–strain relation in the rat (Ref. 27), dog (Ref. 6), or rabbit (Ref. 23) myocardium, and the parameters estimated using the model.

	C (kPa)	b_1	b_2	b_3	b_4 (kPa)	W form
Rat	2.2	9.2	2.0	3.7		Eq. (1)
Dog	1.76	18.5	3.58	1.63		Eq. (1)
Rabbit	0.206	9.13	2.32	0.08		Eq. (3)
Model	1.76	50.0	5.0	1.63	200	Eq. (2)

undeformed state. Note that the material parameters b_1, b_2, and b_3 are unrelated to those in Eq. (1), and typically do not have the same values as in Eq. (1).

The material parameters for the rat[27] and dog[14] are listed in Table 2, along with the parameters reported by Lin and Yin[23] using the strain energy function above [Eq. (3)] and the parameters we propose here. Figure 9 shows the equibiaxial fiber and cross-fiber stress–strain relations.

It has been previously shown that the rat myocardium is significantly less stiff than that of the canine, and that both materials are stiffer in the fiber direction than in the cross-fiber direction.[26] The material parameters proposed here also suggest that rabbit myocardium is stiffer in the fiber direction than in the cross-fiber direction. In addition, our results suggest rabbit myocardium may be stiffer than canine myocardium (note the solid lines are steeper than the dotted lines in Fig. 9).

Gallagher *et al.*[10] noted that strains they measured were lower than those observed in other species, and the material parameters determined here suggest intact myocardium of the rabbit may be stiffer than that in the rat and canine. These results, however, are not completely consistent with the material description of the rabbit myocardium proposed by Lin and Yin,[23] which show nearly equal stiffness in the fiber and cross-fiber directions, and a generally more compliant material at strains below 20%. This discrepancy may be due in part to differences in the experimental preparations: strains obtained from LV passive inflation may be affected by the myocardial laminae, but in thin slabs of tissue this effect would be minimized because the sheets lie transmurally in the ventricle. The specimens used in Lin and Yin[23] were excised at the midwall where the sheets run approximately normal to the epicardial plane.[22] In addition, the passive inflation protocol used by Gallagher *et al.*[10] produced maximal fiber strain on the order of 10%. The thin slabs used in the equibiaxial tests conducted by Lin and Yin were subjected to 30% strain in the fiber or cross-fiber direction. This may have made the tissue more compliant due to strain softening.[9]

Similar to the strain, Cauchy stress resolved in fiber and cross-fiber directions varied regionally throughout

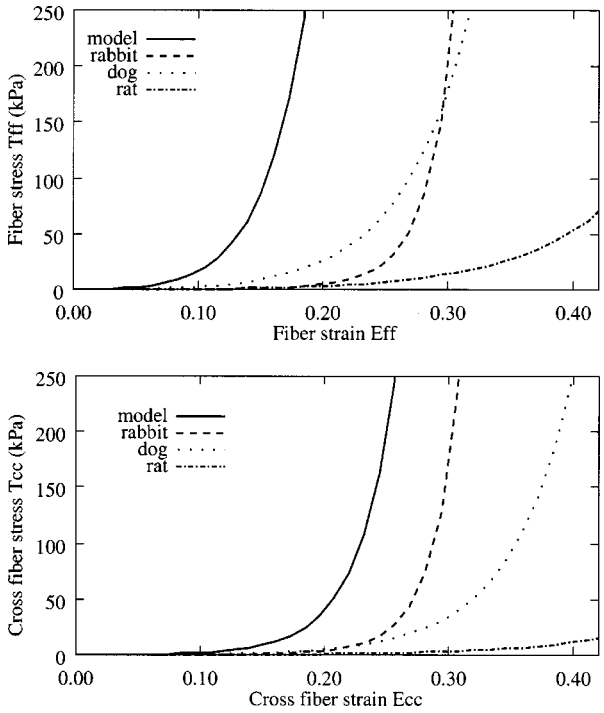

FIGURE 9. Equibiaxial fiber (top) and cross fiber (bottom) stress-strain relations from models of the dog (Ref. 6), rat (Ref. 27), rabbit (Ref. 23) myocardium, and the model described here.

the LV and apex. Negative stresses tended to be located in the highly curved regions near the papillary insertions at the subendocardium, although cross fiber stress was also negative at the midwall near the posterior papillary. The largest variations in both fiber and cross-fiber stress occurred at the subendocardium, where the largest stresses were at the apex, although it is unknown if this actually occurs in the heart. The apex is the thinnest region in the LV[4] and may be a site of high stress, but this has not been experimentally measured. Throughout the entire LV wall and apex the mean fiber stress was higher than the mean cross-fiber stress, suggesting that fiber orientation may play a significant role in the stress distribution in intact myocardium. Aside from this, however, there were no other apparent correlations between stress and fiber orientation.

Limitations

Though this model was anatomically detailed in terms of the geometry and fiber orientations, many features of the heart are still lacking. The model does not include the imbrication angle of the myofibers.[29] By including the imbrication angle in simulations of passive LV inflation, Bovendeerd and co-workers[2] found that shear deformation was significantly reduced in the basal and apical regions of the ventricle. The model lacks the myocardial laminar sheet structure which was first quan-

tified by LeGrice *et al.*[22] and most recently by Costa *et al.*,[7] who showed that sliding and deformation of the myocardial laminae may contribute significantly to systolic thickening of the LV wall and suggested an orthotropic (rather than transversely isotropic) constitutive law may better describe the material properties of LV myocardium. The unloaded reference state for the model contained no residual stress, though residual stress is known to exist in the unloaded heart[7] and reduces transmural cross-fiber strain gradients.[14] Thus the cross-fiber strains reported here may be overestimated.

Numerically optimized material parameters, obtained by minimizing the sum of squared differences between experimental and model-predicted variables, have been determined previously by Guccione *et al.*[14] using a cylindrical model of the LV. They verified that a global minimum had been obtained by repeating their optimization procedure from a wide range of initial parameter values and computing the variance of each parameter. Such an effort can potentially require a very large number of simulations, and the resulting solution may not be unique.[12] From a practical standpoint we chose not to numerically optimize the material parameters given that each simulation required approximately 5 h (and over 230 CPU hours) to complete. We would expect the model to better reproduce the experimental strain measurements had the material parameters been numerically optimized instead of heuristically estimated. Nevertheless, by using the estimated material parameters obtained after 12 simulations, the model reproduced the experimentally measured fiber and cross-fiber strains well within the experimental accuracy.

CONCLUSIONS

We have estimated the material properties of the intact rabbit myocardium using a three-dimensional model of the rabbit ventricles. The parallel computational approach was shown to be highly scalable, reducing the time required to obtain a solution by 90%. Estimated material parameters reproduced the epicardial strains measured previously in the passively inflated rabbit heart. On the epicardium, fiber strain was larger than cross-fiber strain, a feature observed elsewhere in the dog and rat myocardium. Model strains at the midwall and endocardium, although similar to transmural strains observed in the canine ventricle, are conjectural and still require experimental measurements in the rabbit for comparison. The model may serve as a means to integrate the diverse experimental results from the rabbit into a unified model of cardiac function.

ACKNOWLEDGMENTS

The authors are grateful to Dr. Ann Marie Gallagher for discussions regarding her experiments and access to the raw data. Dr. Walt Baxter, Dr. Bill Karlon, and Dr. Reza Mazhari provided helpful technical advice, and Professor Scott Baden provided an introduction to parallel computation. Derrick Sung provided the stress and strain contour maps. This work was supported by NFS Grant No. BES-9634974 and the National Biomedical Computational Resource Grant No. NIH RR08065.

NOMENCLATURE

E_{ij}	Lagrangian Green's strain tensor components
W	strain energy function
x_i	rectangular Cartesian coordinate
$\tilde{n}$	unit vector in the direction of cardiac myofibers
$\tilde{u}$	global solution vector
$\hat{u}$	approximation of $\tilde{u}$
$\mathbf{K}$	global tangent stiffness matrix
σ_{ij}	Cauchy stress tensor components
T_{ij}	second Piola–Kirchhoff stress tensor components
S_i	finite element arc length
I_i	strain invariant
λ, μ, θ	prolate spheroidal coordinates
ξ_i	isoparametric finite element coordinate
b_i, C	passive material parameters
δv	displacement of variable v
$\mathbf{C}$	right Cauchy–Green deformation tensor

REFERENCES

[1] Bovendeerd, P. H., T. Arts, J. M. Huyghe, D. H. van Campen, and R. S. Reneman. Dependence of local left ventricular wall mechanics on myocardial fiber orientation: A model study. *J. Biomech.* 25(10):1129–1140, 1992.

[2] Bovendeerd, P. H. M., J. M. Huyghe, T. Arts, D. H. van Campen, and R. S. Reneman. Influence of endocardial-epicardial crossover of muscle fibers on left ventricular wall mechanics. *J. Biomech.* 27(7):941–951, 1994.

[3] Bovendeerd, P. H., T. Arts, T. Delhaas, J. M. Huyghe, D. H. van Campen, and R. S. Reneman. Regional wall mechanics in the ischemic left ventricle: numerical modeling and dog experiments. *Am. J. Physiol.* 270(39):H398–H410, 1996.

[4] Bradfield, J. W. B., G. Beck, and R. J. Vecht. Left ventricular apical thin point. *Br. Heart J.* 39(7):806–809, 1977.

[5] Costa, K. D. The structural basis of three-dimensional ventricular mechanics. Ph.D. thesis, University of California, La Jolla, CA, 1996.

[6] Costa, K. D., P. J. Hunter, J. M. Rogers, J. M. Guccione, L. K. Waldman, and A. D. McCulloch. A three-dimensional finite element method for large elastic deformations of ventricular myocardium: II—prolate spheroidal coordinates. *J. Biomech. Eng.* 118(4):464–472, 1996.

[7] Costa, K. D., K. May-Newman, D. Farr, W. G. O'Dell, A. D. McCulloch, and J. H. Omens. Three-dimensional residual

strain in midanterior canine left ventricle. *Am. J. Physiol.* 273(42):H1968–H1976, 1997.
[8] Dias da Cunha, R., and T. Hopkins. A parallel implementation of the restarted GMRES iterative algorithm for nonsymmetric systems of linear equations. *Adv. Comput. Math.* 2(3):261–277, 1994.
[9] Emery, J. L., J. H. Omens, and A. D. McCulloch. Biaxial mechanics of the passively overstretched left ventricle. *Am. J. Physiol.* 272(41):H2299–H2305, 1997.
[10] Gallagher, A. M., J. H. Omens, L. L. Chu, and J. W. Covell. Alterations in collagen fibrillar structure and mechanical properties of the healing scar following myocardial infarction. *Cardiovasc. Pathobiol.* 2(1):25–36, 1997.
[11] Gray, R. A., J. Jalife, A. V. Panfilov, W. T. Baxter, C. Cabo, J. M. Davidenko, and A. M. Pertsov. Nonstationary vortex-like reentrant activity as a mechanism of polymorphic ventricular tachycardia in the isolated rabbit heart. *Circulation* 91(9):2454–2469, 1995.
[12] Green, A. E., and J. E. Adkins. Large Elastic Deformations, 2nd ed. Clarendon, Oxford, 1970.
[13] Guccione, J. M., K. D. Costa, and A. D. McCulloch. Finite element stress analysis of left ventricular mechanics in the beating dog heart. *J. Biomech.* 28(10):1167–1177, Oct 1995.
[14] Guccione, J. M., A. D. McCulloch, and L. K. Waldman. Passive material properties of intact ventricular myocardium determined from a cylindrical model. *J. Biomech. Eng.* 113(1):42–55, 1991.
[15] Holmes, J. W., J. A. Nuñez, and J. W. Covell. Functional implications of myocardial scar structure. *Am. J. Physiol.* 272(41):H2123–H2130, 1997.
[16] Hughes, T. J. R., I. Levit, and J. Winget. An element-by-element solution algorithm for problems of structural and solid mechanics. *Comput. Methods Appl. Mech. Eng.* 36:241–254, 1983.
[17] Humphrey, J. D., and F. C. Yin. Constitutive relations and finite deformations of passive cardiac tissue II: stress analysis in the left ventricle. *Circ. Res.* 65(3):805–817, 1989.
[18] Hutchinson, S. A., L. V. Prevost, C. H. T. J. N. Shadidxi, and R. S. Tuminaro. Aztec User's Guide Version 2.0. Sandia National Laboratories, Albuquerque NM 87185, Jul 1998. Available from www.cs.sandia.gov/CRF/pspapers/Aztec_ug_2.0.ps
[19] Huyghe, J. M., T. Arts, D. H. van Campen, and R. S. Reneman. Porous medium finite element model of the beating left ventricle. *Am. J. Physiol.* 262(31):H1256–H1267, 1992.
[20] Huyghe, J. M., D. H. van Campen, T. Arts, and R. M. Heethaar. A two-phase finite element model of the diastolic left ventricle. *J. Biomech.* 24(7):527–538, 1991.
[21] Jones, M. T., and P. E. Plassmann. BlockSolve95 Users Manual: Scalable Library Software for the Parallel Solution of Sparse Linear Systems. Argonne National Laboratory, 9700 South Class Avenue, Argonne IL 60439, Jun 1997; Argonne National Laboratory Report 95/48 (revised June 1997). Available from ftp://info.mcs.anl.gov/pub/BlockSolve95/manual.ps.
[22] LeGrice, I. J., B. H. Smaill, L. Z. Chai, S. G. Edgar, J. B. Gavin, and P. J. Hunter. Laminar structure of the heart: Ventricular myocyte arrangement and connective tissue architecture in the dog. *Am. J. Physiol.* 269(38):H571–H582, 1995.
[23] Lin, D. H. S., and F. C. P. Yin. A multiaxial constitutive law for mammalian left ventricular myocardiumin steady-state barium contracture or tetanus. *J. Biomech. Eng.* 120(4):504–517, 1998.
[24] Nielsen, P. M. F., I. J. LeGrice, B. H. Smaill, and P. J. Hunter. Mathematical model of geometry and fibrous structure of the heart. *Am. J. Physiol.* 260(29):H1365–H1378, 1991.
[25] O'Dell, W. G., and A. D. McCulloch. A novel numerical formulation for modeling tissue compressibility. *Adv. Bioeng.* BED-39:1-2, 1998; Proceedings of the 1998 ASME International Mechanical Engineering Congress and Exposition, 15–20 November 1998, Anaheim, California. Edited by Ajit P. Yoganathan.
[26] Omens, J. H., K. D. May, and A. D. McCulloch. Transmural distribution of three-dimensional strain in the isolated arrested canine left ventricle. *Am. J. Physiol.* 261(30):H918–H928, 1991.
[27] Omens, J. H., D. A. MacKenna, and A. D. McCulloch. Measurement of strain and analysis of stress in resting rat left ventricular myocardium. *J. Biomech.* 26(6):665–676, 1993.
[28] Saad, Y., G.-C. Lo, and S. Kuznetsov. PSPARSLIB Users Manual: A Portable Library of parallel Sparse Iterative Solvers. University of Minnesota, Department of Computer Science, 200 Union Street S. E., Minneapolis, MN 55455, Jan 1998. Available from www.cs.umn.edu/Research/arpa/p_sparslib/psp/DOCS/manual.ps.
[29] Streeter, Jr., D. D. Gross morphology and fiber geometry of the heart. In: Handbook of Physiology, Section 2: The Cardiovascular System, edited by R. M. Berne, Vol. 1, Chap. 4, pp. 61–112. Bethesda, MD: American Physiological Society, 1979.
[30] Vetter, F. J., and A. D. McCulloch. Three-dimensional analysis of regional cardiac function: A model of rabbit ventricular anatomy. *Prog. Biophys. Mol. Biol.* 69(2/3):157–183, 1998.
[31] Waldman, L. K. Multidimensional measurement of regional strains in the intact heart. In: Theory of Heart: Biomechanics, Biophysics, and Nonlinear Dynamics of Cardiac Function, edited by L. Glass, P. Hunter, and A. McCulloch, Chap. 7, pp. 145–174. New York: Springer, 1991.
[32] Wathen, A. J. An analysis of some element-by-element techniques. *Comput. Methods Appl. Mech. Eng.* 74(3):271–287, 1989.
[33] Watkins, M. W., B. K. Slinker, Y. Goto, and M. M. LeWinter. 2,3-Butanedione monoxime increases contractile efficiency in the rabbit ventricle. *Am. J. Physiol.* 263(32):H1811–H1818, 1992.
[34] Yeckel, A., and J. J. Derby. Parallel computation of incompressible flows in materials processing: Numerical experiments in diagonal preconditioning. *Parallel Comput.* 23(9):1379–1400, 1997.
[35] Yin, F. C. P., C. C. Chan, and R. M. Judd. Compressibility of perfused passive myocardium. *Am. J. Physiol.* 271(40):H1864–H1870, 1996.